Anal. Chem. **2006,** *78,* 1425−1434

Continuous Flow Microfluidic Demixing of Electrolytes by Induced Charge Electrokinetics in Structured Electrode Arrays

Felix C. Leinweber,* Jan C. T. Eijkel, Johan G. Bomer, and Albert van den Berg

MESA+ Institute for Nanotechnology, BIOS/ Lab-on-a-Chip Group, University of Twente, P.O. Box 217, 7500 AE Enschede, The Netherlands

A continuous flow microfluidic demixing process is realized. It utilizes high external electrical fields that are applied over electrically floating noble metal electrodes in an otherwise straight microchannel. The process converts axial electrical potential gradients into lateral molecular selective transport via a structure oriented ensemble of numerous electrodes. While the individual electrodes locally modify the electrolyte distribution by nonlinear electrokinetic effects and concentration polarization, the directed orientation of the electrode array combines the individual polarization zones to a dedicated molecular enrichment against the generated concentration gradient. A homogeneously concentrated electrolyte can be separated into arbitrarily shaped laminae of increased and depleted concentration by the presented microfluidic demixer.

Microfluidic devices have gained increased interest in many technological applications such as chemical analysis, biotechnology, or medical diagnostics.[1−3] Their attractiveness grounds on several inherent advantages of miniaturization such as the complex integration of different analytical steps, a massive parallelization, a reduced analysis time, or the minimized sample consumption. One of the key features for a successful realization of lab-on-a-chip systems therefore remains the ability to precisely handle microscale liquid-phase volumes. In comparison to conventional microscale or capillary-scale liquid systems, the practical absence of any moving mechanical parts hampers, on one hand, the efficient downscaling of approved conventional approaches but, on the other hand, directs research on new system designs.

One active field of research in microliquid handling has therefore been the development of different types of microfluidic mixers. The confined geometrical dimensions of microfabricated channel systems result in low Reynolds numbers and a laminar flow profile.[4] To enable efficient lateral mixing, different approaches have been chosen to achieve a molecularly homogeneous solution in a reasonable amount of time. These microfluidic mixers reduce either the diffusional path length by filing incoming streams into different laminae, add three-dimensional advective flow component, or induce convection by electrical or mechanical energy input.[5−12] Their common feature remains that all these systems act within the natural direction of the mixing process as defined by an entropy gain for the completely mixed solution. It is therefore not surprising that none of the micromixers allows, if operated in the opposite direction, a demixing of a homogeneously concentrated solution. Thus, the reversion of the entropy-controlled process of mixing into demixing turns out to be a much more complicated problem.

Demixing denotes the reversion of the thermodynamically spontaneous process of mixing. It stringently necessitates an external energy input in order to compensate the entropy decrease during the selective accumulation of a specific compound or material.[13] Common large-scale purification processes realize demixing in technologies such as fractionated distillation, electrodialysis, or reversed osmosis. Benefiting from the advanced microfabrication technologies, the microfluidic approach offers distinct advantages for the miniaturization of purification processes. The ability to apply several different electrical, chemical, or other potential gradients independently from each other over a small spatial area constitutes a major improvement. Via the complex integration of different driving forces, several miniaturized separation and purification techniques in continuous flow format have been successfully realized.[14−17] Microsystem technology still provides another unique feature, namely, the possibility

* To whom correspondence should be addressed. Phone: +31 (0)53 489 5653. Fax: +31 (0)53 489 3595. E-mail: BIOS@utwente.nl.

(1) Oosterbroek, R. E., van den Berg, A., Eds. *Lab-on-a-Chip: Miniaturized Systems for (Bio) Chemical Analysis* and Synthesis; Elsevier: Amsterdam, 2003.
(2) Ehrfeld, W.; Hessel, V.; Löwe, H. *Microreactors*; Wiley-VCh: Weinheim, 2000.
(3) Andersson, H.; van den Berg, A. *Lab-on-Chips for Cellomics*; Kluwer Academic Publishing: Berlin, 2004.
(4) Probstein, R. F. *Physiochemical Hydrodynamics*, 2nd ed.; John Wiley & Sons: New York, 1994.
(5) Bessoth, F. G.; deMello, A. J.; Manz, A. *Anal. Commun.* **1999**, *36*, 213−215.
(6) Veenstra, T. T.; Lammerink, T. S. J.; Elwenspoek, M. C.; van den Berg, A. *J. Micromech. Microeng.* **1999**, *9*, 199−202.
(7) He, B.; Burke, B. J.; Zhang, X.; Zhang, R.; Regnier, F. E. *Anal. Chem.* **2001**, *73*, 1942−1947.
(8) Stroock, A. D.; Dertinger, S. K. W.; Ajdari, A.; Mezic, I.; Stone, H. A.; Whitesides, G. M. *Science* **2002**, *295*, 647−651.
(9) Johnson, T. J.; Ross, D.; Locascio, L. E. *Anal. Chem.* **2002**, *74*, 45−51.
(10) Lin, C. H.; Fu, L. M.; Chien, Y. S. *Anal. Chem.* **2004**, *76*, 5265−5272.
(11) Burghelea, T.; Segre, E.; Bar-Joseph, I.; Groisman, A.; Steinberg, V. *Phys. Rev. E* **2004**, *69*.
(12) Yaralioglu, G. G.; Wygant, I. O.; Marentis, T. C.; Khuri-Yakub, B. T. *Anal. Chem.* **2004**, *76*, 3694−3698.
(13) Kondepudi, D.; Prigogine, I. *Modern Thermodynamics: From Heat Engines to Dissipative Structures*; John Wiley & Sons: Chichester, 1998.
(14) Raymond, D. E.; Manz, A.; Widmer, H. M. *Anal. Chem.* **1994**, *66*, 2858−2865.

10.1021/ac051615n CCC: $33.50
Published on Web 01/25/2006

of freely adjusting the channel geometry. This characteristic enables the incorporation of devised aspects of broken symmetry into microfluidics.[18,19] Consequently, several so far unknown purification processes have been realized.[20−23] Unfortunately, most of them only apply to particles or geometrically extended macromolecules.

In contrast to these particle separation processes, which fail if applied to low molecular weight compounds, we describe in this report a continuous flow microfluidic demixing process that enables the specific lateral displacement of any low molecular weight electrolytes against the concentration gradient. The key feature of this process is the direct conversion of axial energy input into lateral selective transport via the orientation-directed symmetry of the device architecture. The microfluidic demixing systems is based on the nonlinear electrokinetic effects at charged interfaces which are polarized but to not show surface reactions (for an overview see ref 24 and references therein).

So far, a major part of nonlinear or nonequilibrium electrokinetics is related to hierarchically structured porous media and describes the phenomena of electroosmosis and electrophoresis of the second kind.[24−30] The astonishing properties of these effects due to concentration polarization, flow instabilities, and local transport modification have recently been exploited to drastically raise the performance of electrochromatographic separations[31−33] and microfluidics[34−36] as well as to enhance the throughput of electrodialysis.[37−41] But nonlinear electrokinetic effects are not stringently related to porous ion-permselective materials, they also occur around electrically floating electrodes when subjected to external electrical fields. The physiochemical fundamentals of these nonlinear (or induced-charge) electrokinetics at floating electrodes and their hydrodynamic consequences have been the subject of intensive research.[42−49] But the impact of these nonlinear electrokinetic phenomena on the ionic concentration distribution beyond the electrical double layer has been completely out of focus.

In the present article, the conceptual fundamentals of nonlinear electrokinetic concentration manipulation are derived. It will be demonstrated how external electrical fields induce nonequilibrium electrical double layers and what electrochemical surface properties have to be fulfilled. Thereafter, the importance of the hierarchically structured electrode geometry will be discussed: first, on the single-electrode level in order to realize concentration polarization and, second, within the complete electrode ensemble to enable a patterning of the concentration distribution by electrohydrodynamic interactions between the polarization zones and the hydrodynamic flow. Finally, the practical realization of such a microfluidic demixer that meets all these requirements will be demonstrated. A lateral concentration segmentation becomes possible by means of axial electrical fields only whereby the final patterns remain a function of the structure of the electrode array only.

EXPERIMENTAL SECTION

Microchip Fabrication. The microfluidic devices were fabricated by standard photolithographic and wet-etching processes.[50] Two Pyrex 7740 glass wafers of 0.5-mm thickness (Sensor Prep Sciences) were used. While the top wafer contained the noble metal electrode array as well as the access holes for the electrolyte reservoirs, the bottom wafer holds the microfluidic channel. This allows free optical access for fluorescence intensity probing by use of an inverted microscope. In the first step of the fabrication process, the carefully cleaned top wafer was sputtered with a 20-nm adhesion layer of titanium followed by a 150-nm gold layer. After deposition and the photolithographic development of a positive photoresist, the electrode array was structured by wet-etching to realize electrode dimensions of 50 μm in axial extension and 20 μm in lateral width. Thereafter, the connection holes for the electrolyte reservoirs were fabricated on the same wafer but from the other side by powder-blasting.[51] The second part of the process consisted of etching the 250-μm-wide nanofluidic channel with 1000 nm in maximum height into the bottom wafer by standard BHF wet-etching techniques. The channel height was kept at the submicrometer range since a reasonable low ratio between electrode and channel height had to be kept while

(15) Tokeshi, M.; Minagawa, T.; Kitamori, T. *Anal. Chem.* **2000**, *72*, 1711−1714.
(16) Macounová, K.; Cabrera, C. R.; Yager, P. *Anal. Chem.* **2001**, *73*, 1627−1633.
(17) Lilliehorn, T.; Simu, U.; Nilsson, M.; Almqvist, M.; Stepinski, T.; Laurell, T.; Nilsson, J.; Johansson, S. *Ultrasonics* **2005**, *43*, 293−303.
(18) Astumian, R. D. *Science* **1997**, *276*, 917−922.
(19) Ajdari, A. *Phys. Rev. E* **2000**, *61*, R45−R48.
(20) Han, J.; Turner, S. W.; Craighead, H. G. *Phys. Rev. Lett.* **1999**, *83*, 1688−1691.
(21) Matthias, S.; Müller, F. *Nature* **2003**, *424*, 53−57.
(22) Huang, L. R.; Cox, E. C.; Austin, R. H.; Sturm, J. C. *Science* **2004**, *304*, 987−990.
(23) Chiou, P. Y.; Ohta, A. T.; Wu, M. C. *Nature* **2005**, *436*, 370−372.
(24) Dukhin, S. S. *Adv. Colloid Interface Sci.* **1993**, *44*, 1−134.
(25) Dukhin, S. S.; Mishchuk, N. A.; Zholkovskii, E. K. *Colloid J. USSR* **1987**, *49*, 761−769.
(26) Dukhin, S. S.; Mishchuk, N. A. *Colloid J. USSR* **1989**, *51*, 570−581.
(27) Mishchuk, N. A.; Dukhin, S. S. *Colloid J. USSR* **1990**, *52*, 427−431.
(28) Dukhin, S. S. *Adv. Colloid Interface Sci.* **1991**, *35*, 173−196.
(29) Mishchuk, N. A.; Takhistov, P. V. *Colloids Surf. A* **1995**, *95*, 119−131.
(30) Barany, S. *Adv. Colloid Interface Sci.* **1998**, *75*, 45−78.
(31) Leinweber, F. C.; Tallarek, U. *Langmuir* **2004**, *20*, 11637−11648.
(32) Nischang, I.; Tallarek, U. *Electrophoresis* **2004**, *25*, 2935−2945.
(33) Tallarek, U.; Leinweber, F. C.; Nischang, I. *Electrophoresis* **2005**, *26*, 391−404. Leinweber, F. C.; Tallarek, U. *J. Phys. Chem. B* **2005**, *109* (46), 21481−21485.
(34) Wang, S. C.; Lai, Y. W.; Ben, Y.; Chang, H.-C. *Ind. Eng. Chem. Res.* **2004**, *43*, 2902−2911.
(35) Foote, R. S.; Khandurina, J.; Jacobson, S. C.; Ramsey, J. M. *Anal. Chem.* **2005**, *77*, 57−63.
(36) Wang, Y.-C.; Stevens, A. L.; Han, J.-Y. *Anal. Chem.* **2005**, *77*, 4293−4299.
(37) Rubinstein, I.; Maletzki, F. *J. Chem. Soc., Faraday Trans. 2* **1991**, *87*, 2079−2087.
(38) Mishchuk, N. A. *Desalination* **1998**, *117*, 283−295.
(39) Rubinstein, I.; Zaltzman, B. *Phys. Rev. E* **2000**, *62*, 2238−2251.
(40) Vasil′eva, V. I.; Shaposhnik, V. A.; Grigorchuk, O. V.; Malykhin, M. D. *Russ. J. Electrochem.* **2002**, *38*, 846−852.
(41) Ibanez, R.; Stamatialis, D. F.; Wessling, M. *J. Membr. Sci.* **2004**, *239*, 119−128.
(42) Dukhin, S. S.; Shilov, V. N. *Adv. Colloid Interface Sci.* **1980**, *13*, 153−195.
(43) Dukhin, S. S.; Murtsovkin, V. A. *Colloid J. USSR* **1986**, *48*, 203−209.
(44) Gamayunov, N. I.; Murtsovkin, V. A.; Dukhin, S. S. *Colloid J. USSR* **1986**, *48*, 197−203.
(45) Gamayunov, N. I.; Mantrov, G. I.; Murtsovkin, V. A. *Colloid J. USSR* **1992**, *54*, 20−23.
(46) Murtsovkin, V. A. *Colloid J. Russ. Acad. Sci.* **1996**, *58*, 341−349.
(47) Bazant, M. Z.; Thornton, K.; Ajdari, A. *Phys. Rev. E* **2004**, *70*, Art. No. 021506.
(48) Bazant, M. Z.; Squires, T. M. *Phys. Rev. Lett.* **2004**, *92*, 066101.
(49) Squires, T. M.; Bazant, M. Z. *J. Fluid Mech.* **2004**, *509*, 217−252.
(50) Madou, M. J. *Fundamentals of Microfabrication*; CRC Press: Boca Raton, FL, 2001.
(51) Guijt, R. M.; Baltussen, E.; van der Steen, G.; Schasfoort, R. B. M.; Schlautmann, S.; Billiet, H. A. H.; Frank, J.; van Dedem, G. W. K.; van den Berg, A. *Electrophoresis* **2001**, *22*, 235−241.

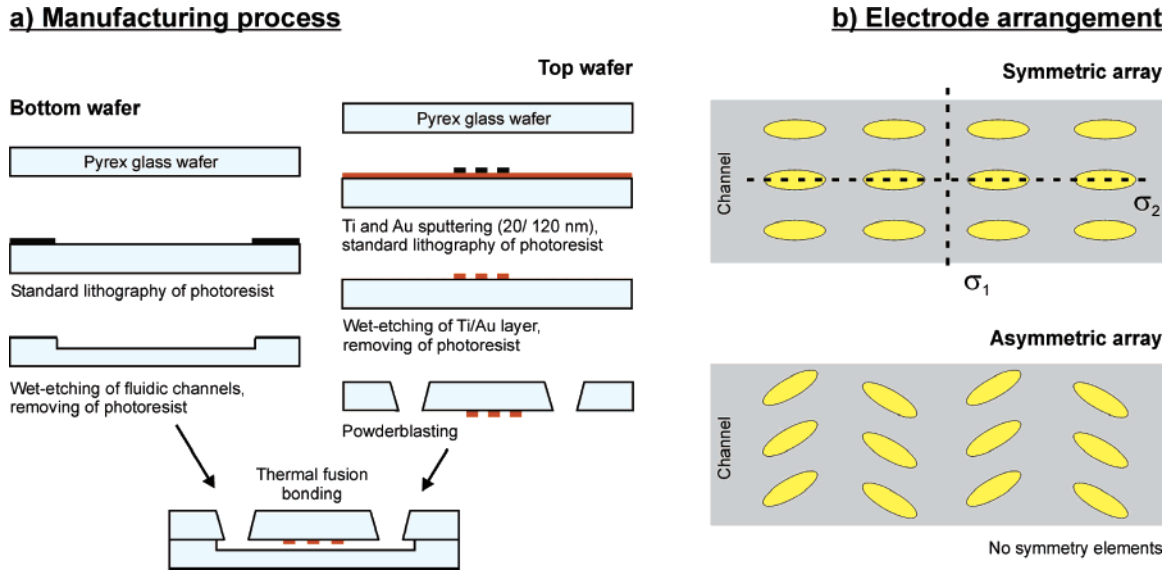

Figure 1. (a) Photolithographic fabrication of the microfluidic device with different electrode geometries. The system was designed for use in an inverted fluorescent microscope with the electrode array and the electrolyte reservoirs in the top wafer and the microfluidic channel system etched into the bottom wafer. (b) Symmetry-oriented design of the electrode array. Symmetric arrays offer at least one symmetry element, whereas asymmetric arrays do not.

relatively good optical detectability was maintained. After carefully cleaning and activating the glass surfaces, both wafers were sealed by thermal bonding for 1 h at 650 °C. Finally, the raw wafer was diced into 1.5 × 2.0 cm pieces in order to fit into the chip holder. A schematic view of the production process is depicted in Figure 1.

Experimental Realization. The microfluidic devices were inserted into a specialized chip holder that allows the precise placement into the *xyz*-tuning stage of an inverted laser microscope. This chip holder consisted of a ground and a cover plate that were both fabricated from poly(vinyl choride), a chemically inert, electrically nonconductive, and mechanically stable polymer. High-voltage electrical energy supply was accomplished by a Keithley 2410 source meter (Keithley Instruments). This instrument is capable of generating dc voltages up to 1100 V and can be operated either manually or computer controlled. Finally, the whole microscope system was carefully grounded against electrical discharge.

Fluorescence intensity probing was carried out with a Leica DM IRM inverted epifluorescence microscope (Leica Microsystems). The microscope consisted of a 10×/0,38 NA epiplan objective with a high optical field depth and filter settings for 488-nm excitation and long-pass detection. For illumination, three different light sources were available and could be operated depending on the channel depth and the fluorescent tracer concentration: (i) a tungsten lamp, (ii) a 100-W mercury vapor lamp, and (iii) a 30-mW solid-state laser at 488 nm (Coherent Technologies). The microscope system was equipped with a highly sensitive Orca ER CCD camera (Hamamatsu). Data acquisition and camera control were accomplished with the Wasabi control software delivered by Hamamatsu. The camera's exposure time and signal amplification were set to keep the fluorescence signal within the linear range. Thus, the fluorescence intensity can be quantitatively related to the local tracer concentration. Postexperimental data processing was carried out with the software package ScionImage, freely available at www.scioncorp.com.

The fluidic phase consisted of an aqueous solution of sodium phosphate buffer at pH 7.0 with concentrations ranging from 10^{-4} to 10^{-1} M for the charged dyes and of a 90:10 = DMSO:water solution of equal buffer concentration for the electroneutral fluorescent molecule. Different fluorescent dyes were used: the twice negatively charged Bodipy-disulfonate and the electroneutral Bodipy 493/503 (both from Molecular Probes) and the singly positive charged Rhodamine 6G (Sigma-Aldrich). These dyes were used as tracer compounds in a concentration of 10^{-5} mol/L in order to remain at least 1 order of magnitude below the ionic strength determining buffer concentration.

Cyclic voltammetry was carried out on the computer-controlled Parstat 2263 potentiostat (Princeton Applied Research) with the aid of a home-built conductivity cell. The reference electrode was an $Ag/AgCl/KCl_{sat}$ electrode (Radiometer Analytical) with a fixed potential at 0.197 V.

RESULTS AND DISCUSSION

Nonlinear Electrokinetic Properties. The explanation of the presented demixing process is based on nonlinear electrokinetic effects around electrically floating electrodes without considering Faradaic processes. Rather than focusing on the pure hydrodynamics such as flow velocity or possible recirculating vortices, the current work exploits these nonlinear electrokinetics for the manipulation of the ionic concentration distribution. Three main physical properties lead to the desired electrohydrodynamic concentration manipulation: (i) the electrokinetic induction of nonequilibrium double layers and strong surface conductivity into the electrically floating noble metal electrodes, (ii) ion-permselective surface flux and concentration polarization, and (iii) convective flow through the structured geometry of an ensemble of many electrodes. These characteristics will now be discussed in detail.

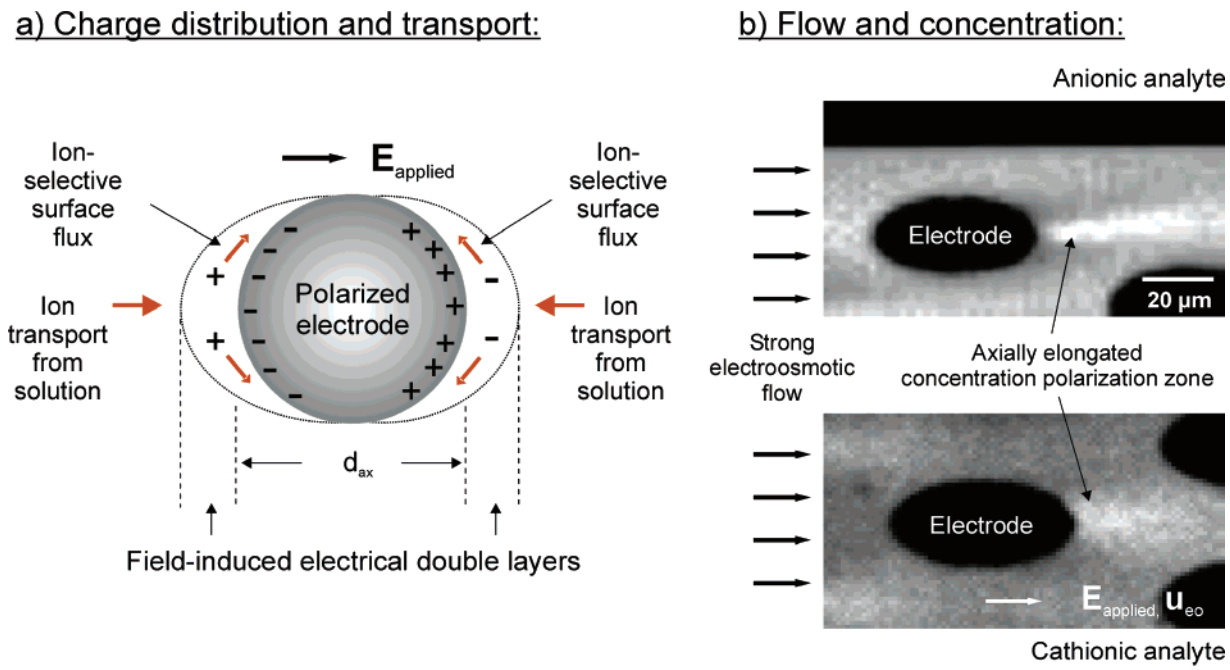

Figure 2. (a) Schematic description of the axial potential distribution and local transport properties at electrically floating electrodes under application of external electrical fields. Nonequilibrium electrical double layers with a field-dependent surface potential $\Phi_0 = d_{ax}E/2$ are induced, with d_{ax} denoting the axial extension of the electrode and E the electrical field strength. The electrodes are considered blocking; i.e., no Faradaic surface reactions occur. (b) Concentration distribution and concentration polarization around a single floating electrode at 44 kV/m. The Dukhin number calculates to 3000. The conditions are described in the Experimental Section.

When external electrical fields are applied over electrically floating electrodes, the conductive material acts as an electrical short circuit that leads to a dynamic rearrangement of the electron density distribution inside this material to guarantee a constant internal electrical potential. As a consequence, the electrodes' polar solid−liquid interfaces become polarized by space charges of increased and reduced electron density (Figure 2a). The compensation of these space charges involves the attraction of counterions from the electrolyte solution. Field-induced double layers develop. Due to their origin in a charge distribution far from the equilibrium value, which is obtained without any externally applied fields, they are also called nonequilibrium electrical double layers.[52] While the physical structure of these nonequilibrium double layers remains identical to those at interfaces with a fixed surface charge density, the big difference grounds in the electrical potential decay normal to the surface, which is characterized by a strong dependence on the applied electrical field strength. The surface potential ϕ_0 scales linearly with the external field strengths (cf. legend of Figure 2), but consequently, the electrokinetic properties are also field-dependent. To determine the electrical potential at the outer Helmholtz plane ϕ_1, which can be regarded as an indicator for the ζ-potential, the surface charge density in the solid part of the interface has to be equaled by the charge density in the adsorbed and diffuse electrical double layer. Especially the knowledge of ϕ_1 is of decisive importance because the field dependence of the expected nonlinear effects will mainly show a strong correlation with this electrokinetically fundamental potential and its field dependency.

The equation for the determination of ϕ_1 combines according to the fundamental Stern model of charged interfaces to[53,54]

$$\frac{\epsilon(\phi_0 - \phi_1)}{\delta} = \frac{FZ}{2 + \left(\frac{18}{c}\right)e^{-F\phi_1/RT}} - \frac{FZ}{2 + \left(\frac{18}{c}\right)e^{F\phi_1/RT}} + \frac{1}{2}\sqrt{\frac{10^3 c\epsilon RT}{18}}\,\mathrm{Sinh}\left(\frac{F\phi_1}{2RT}\right) \quad (1)$$

where ϵ denotes the permittivity and $\delta \approx 330$ pm, the assumed thickness of a monolayer of charge carriers inside the solid part of the interface. F, R, and T are the Faraday constant, the gas constant, and the absolute temperature; Z is the maximum monolayer adsorption of $\sim 1.7 \times 10^{-5}$ mol/m^2 and c the molar concentration. The numerical solution was carried out by least-squares optimization routines. As demonstrated by the numerical results, the potential at the outer Helmholtz plane shows a sigmoidal field dependence with a strong increase at low induced surface potentials whereas an asymptotic behavior at high field strengths is observed (Figure 3a). Thus, a strong nonlinearity of the nonequilibrium electrokinetic effect is expected up to moderate external field strengths while at high electrical fields an asymptotic behavior toward a linear dependence seems to be likely.

The knowledge of the electrical potential distribution inside the nonequilibrium double layer alone remains insufficient to describe the demixing of electrolytes. First, surface conductivity, a physical property relating the electrical potential with the ionic concentration distribution,[55] has to be quantified. Since the

(52) Lyklema, J. *Fundamentals of Interface and Colloid Science, Vol. II: Solid−Liquid Interfaces*; Academic Press: San Diego, CA, 1995.

(53) Stern, O. *Z. Elektrochem.* **1924**, *30*, 508−516.
(54) Grahame, D. C. *Chem. Rev.* **1947**, *41*, 441−501.

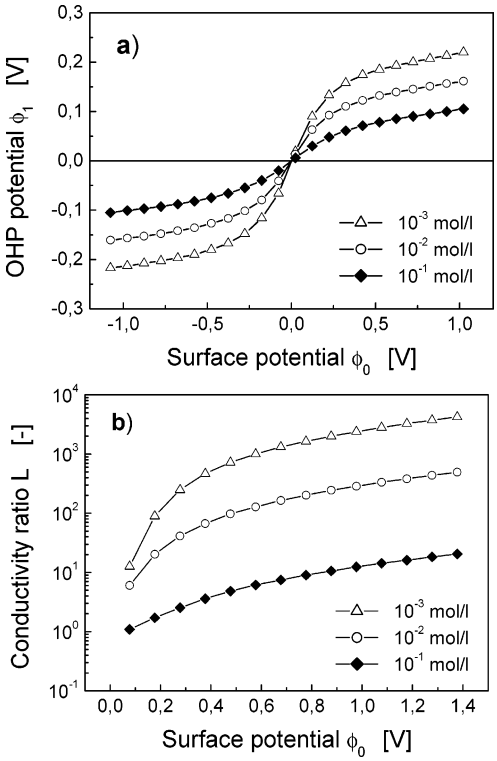

Figure 3. (a) Numerical calculation of the electrical potential Φ_1 at the outer Helmholtz plane (OHP) vs the field-induced surface potential Φ_0. The calculation were carried out according to the Nernst model of the electrical double layer.[53] (b) Dependence of the dimensionless conductivity ratio L between surface and bulk conductivity on the surface potential Φ_0.

nonequilibrium double layer is conventionally built up by a layer of adsorbed and a zone of diffuse counterions, the overall surface conductivity can be considered as the sum of the conductivities from both parts.[55] For a monovalent and symmetric electrolyte with equal diffusivities, the overall surface conductivity becomes calculated by the conductivities inside both the adsorbed and diffuse double layer by

$$\kappa_s = \kappa_s^i + \kappa_s^d \tag{2a}$$

$$\kappa_s^i = \sigma^i(\phi_1)\mu^i \tag{2b}$$

$$\kappa_s^d = 2Fc\lambda_D\mu^i(1 + 3m)\ \mathrm{Cosh}(F\phi_1/RT) \tag{2c}$$

λ_D is the Debye length, $\sigma^i(\phi_1)$ and μ^i denote the surface charge density (a function of ϕ_1) and the electrophoretic mobility inside the Helmholtz plane, and m is a constant factor depending on the electrolyte. The data for the bulk electrolyte, e.g., diffusivity D^i and electrophoretic mobility μ^i for the sodium phosphate buffer, were taken from a standard reference book.[56]

Since in terms of the intended demixing effect a strong effect of the field-induced surface properties on the bulk electrolyte concentration is desired, the conductivity ratio between surface and bulk conductivity constitutes the decisive measure. This assumption is in contrast to the existing literature, where usually the dimensionless Dukhin number is used for a quantitative measure of nonlinear phenomena.[52] The reason for this change is the main drawback of the Dukhin number: in that case, the axial extension constitutes the decisive quantity to explain the dependence of the surface conductivity on the applied electrical field strength. As explained above by the theoretical considerations on the Stern model of the electrical double layer, the surface potential scales linearly with the applied field strength but surface conductivity scales in a complex nonlinear way. Therefore, the introduction of the conductivity ratio with its strong nonlinear dependence on the applied field strength now allows the more detailed explanation of nonlinear effects at higher field strengths. Therefore, in the current work, the Debye length is the decisive axial length scale. If this measure is used, it becomes possible to quantitatively relate the amount of mobile charge carriers inside the electrical double layer to those within the bulk electrolyte solution because the volumetric charge density of the double layer becomes approximated. This gives then a real conductivity ratio.

But the use of the pure axial extension of the electrodes as it is done for the Dukhin number fails for a second reason. The nonlinear effects scale nonlinearly with the applied electrical field as shown by the ϕ_0 versus ϕ_1 data whereas the Dukhin number scales linearly with the applied field. This would imply a steady increase of the nonlinear effects with the applied fields and no deviation from the nonlinearity. However, the present data prove asymptotic behavior for high electrical field strengths (Figure 3a and data below). Thus, the determination of the conductivity ratio L by the following expression remains more meaningful with respect to the numerical calculation of the electrokinetically active double layer potentials and the experimental observations of the nonlinear effects. The conductivity ratio L is then derived by

$$L = \kappa_s/\lambda_D\kappa_{el} \tag{3}$$

whereby λ_D denotes the Debye length. The numerical determination of dimensionless number indicates that especially low ionic strength electrolytes and high electrical field strengths strongly favor surface over bulk conductivity (Figure 3b). Again, an asymptotic behavior at high induced surface potentials is observed. Since this conductivity ratio summarizes the possible effects of surface conductivity on the bulk ionic concentration distribution, the most pronounced nonlinear electrokinetic effects are expected under conditions of high dimensionless numbers.

The physical property of surface conductivity, however, only summarizes the field-induced modifications of the ionic concentration distribution inside the electrical double layer with a spatial extension of only some tens of nanometers in maximum. This magnitude is, of course, insufficient to enable an efficient manipulation of the ionic concentration inside the bulk electrolyte solution at a distance of several tens to hundreds of micrometers from the solid−liquid interface. Therefore, additional mechanisms have to account for the desired long-range concentration manipulation. These mechanisms are the modifications of the local transport properties due to the ion-permselective character of the field-induced electrical double layer. If a net transport through this ion-selective domain is realized, the local electrical field

(55) Lyklema, J.; Minor, M. *Colloids Surf. A* **1998**, *140*, 33−41.
(56) Lide, D. R. *CRC Handbook of Chemistry and Physics*; CRC Press: Boca Raton, FL, 1997.

strengths as well as the ionic concentration become dynamically altered and constitute the basis for the desired demixing of electrolytes.

To realize these mechanisms, surface conductivity has to be first converted into an ion-selective surface flux density by electrode surfaces that are tilted with respect to the applied electrical potential gradient. In these cases, a tangential Coulomb force acts on the counterions within the double layer and moves them along the electrode surface (cf. Figure 2a, where the transport mechanisms are schematically drawn for curved electrodes). The local transport properties become significantly altered as compared to the case of a straight open tubular capillary in order to keep the continuity of mass and charge flux. Since the strong ion-selective transport inside the double layer can only be replenished by diffusional transport from the surrounding electrolyte solution, a concentration gradient close to the double layer develops. This leads to a dynamic modification of the concentration distribution in the surrounding electrolyte, a phenomenon that is also called concentration polarization.

The mechanism of the occurrence of concentration polarization in close vicinity to the ion-permselective double layer is identical to that around ion-exchange membranes in electrodialysis. A detailed discussion of the underlying transport phenomena can be found in the seminal reference book of Friedrich Helfferich.[57] But in contrast to membranes with their tortuous interior pore space, which hinders an efficient counterionic transport,[58] the conductivity ratio for the present experimental conditions and the case of a single electrical double layer strongly favors the transport inside the ion-selective domain. In such cases, the concentration gradient from the concentration in the bulk electrolyte remains insufficient to enable the ionic transport into the ion-selective domain. Consequently, the concentration becomes dynamically increased to guarantee the continuity of mass flux. Thus, under conditions of conductivity ratios, polarization zones with strongly increased ionic concentration develop. The quantitative fluorescence image of the ionic concentration distribution around a single floating electrode at elevated dimensionless conductivity numbers proves the development of the above-described concentration polarization with increased ionic concentration (Figure 2b).

The observed concentration patterns indicate that the ionic concentration distribution around the electrodes shows a strong anisotropy with respect to the flow direction. In front of the electrodes hardly any concentration polarization can be detected whereas behind the electrodes the polarization extends over several tens of micrometers. The observed anisotropy of the concentration polarization indicates the existence of electrohydrodynamic interactions between the hydrodynamic flow and the electrokinetically induced concentration patterns. While at the frontal side of the electrodes, strong convective flow prevails directly to the electrode surface, the downstream area is characterized by strongly reduced convective flow.[4] Therefore, in this geometrically extended slipstream of the electrodes, concentration polarization can well develop. Additionally, the polarization zones can be patterned by the flow field because the basic physical property of concentration polarization is that the zones are electroneutral and therefore not tightly bound by electrostatic forces to the solid−liquid interface as the electrical double layers do.[57] Their exact extension strongly depends on the hydrodynamic flow properties around the ion-selective domain as known from membrane science.[59] There exist definite interactions with the hydrodynamic flow field along the membranes that lead to a spatial deformation of the concentration polarization zones. This means that the hydrodynamic conditions can be used to shape the size of the concentration polarization zones. They can either be reduced in their thickness, as it is the case in electrodialysis, or they can be elongated for the desired demixing purpose. Thus, these interactions between hydrodynamic flow and electrokinetic concentration manipulation provide the desired mechanism to manipulate the bulk ionic concentration distribution far beyond the electrical double layer and constitute the basis for the presented electrohydrodynamic demixing process.

Surface Electrochemistry of Electrodes. Under the present high electrical field strengths of several tens of kilovolts per meter, the field-induced potential difference between the electrode surface and the electrolyte may easily reach several hundred millivolts (cf. the legend of Figure 2; the surface potential scales linearly with the applied field strength). This electrical potential difference is sufficient enough to enable electrochemical surface reactions, for example, by buffer or analyte decomposition, electrode corrosion, or water dissociation.[60] Since Faradaic surface reactions are generally accompanied by ion fluxes normal to the surface, their occurrence would impede the evolution of the above-mentioned tangential transport inside the double layer and the desired concentration polarization effects. Thus, the question has to be answered whether the dynamic rearrangement of the electron density inside the floating electrodes is accompanied by any electrochemical surface reactions or whether the electrodes stay blocking in the sense of being purely capacitatively charged.

The existence of possible electrochemical reactions at the electrode surface was probed by cyclic voltammetry.[61] Since it is quite impossible to electrochemically probe the existence of surface reactions at the surfaces inside the microfluidic device, two reference wafers of exactly the same surface properties were used. Instead of having microstructured electrodes, their surface was completely covered with the electrode material in order to guarantee enough surface area for the electrochemical experiments. The preparation conditions of these two reference wafers were exactly the same as during the microchip fabrication, whereby one wafer was additionally subjected to the 1-h thermal treatment as applied during fusion bonding. Especially this treatment is of major importance because the heating enables the less noble metal atoms of the adhesion layer to diffuse into the above sputtered noble metal electrode material. This may alter the electrochemical surface properties of the complete electrode. The voltammetry data of the two titanium−gold working electrodes were recorded in contact with a degassed sodium phosphate buffer and the fluorescent dye (Figure 4a). Obviously, the electrode material does not show any corrosive oxidation reactions nor does there seem to be any buffer decomposition processes. The only reversible electrochemical reactions that can be moni-

(57) Helfferich, F. *Ion Exchange*; McGraw-Hill Book Co.: New York, 1962.
(58) Samec, Z.; Trojanek, A.; Samcova, E. *J. Phys. Chem.* **1994**, *98*, 6352−6358.
(59) Tanaka, Y. *J. Membr. Sci.* **1991**, *57*, 217−235.
(60) Pickett, D. J. *Electrochemical Reactor Design*; Elsevier: Amsterdam, 1977.
(61) Bard, A. J.; Faulkner, L. R. *Electrochemical Methods*; John Wiley & Sons: New York, 1980.

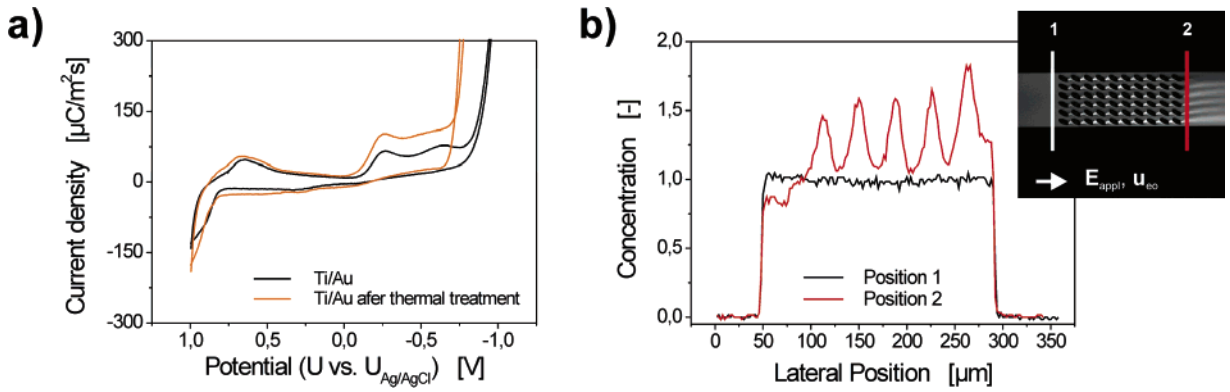

Figure 4. (a) Cyclic voltammetry of the titanium/gold electrode material. The electrolyte solution was a 10 mM sodium phosphate buffer at pH 7.0 with 10^{-4} M fluorescent dye. The scanning range 1 V/−1 V/+1 V was chosen to represent best the electrochemical conditions inside the microfluidic device. (b) Fluorescent images and lateral concentration profiles of a pH-insensitive dye at an electrical field strength of 24 kV/m showing strong concentration effects. The electrical potential drop of maximum 1 V over the electrodes is below the water dissociation potential difference. Faradaic reactions due to electrolytic reaction of water can be ruled out for the present electrolyte system.

tored are water dissociation at high anodic and cathodic potentials. Additionally, despite a thorough degassing of the buffer solutions, the reduction of traces of oxygen dissolved in water and of oxygen adsorbed to the surface could be detected for both types of working electrodes (at 0.7 and −0.25 V vs $U_{Ag/AgCl}$).[61] Besides a slightly reduced overpotential for hydrogen generation, the titanium/gold electrode after thermal treatment shows nearly the same electrochemical properties as the same electrode before the heat exposition. These data indicate that even after the thermal treatment the titanium/gold electrode remains electrochemically inert and surface reactions only occur for traces of dissolved oxygen and, of course, for water dissociation. Thus, since water dissociation needs a potential difference of at least 1.23 V, of kinetic hindrance by overpotentials is not taken into account, the electrodes can be assumed being capacitatively charged.

However, corresponding to literature on nonequilibrium electrokinetics around electrically floating metal domains in strong electrical fields, electrochemical surface reactions might also be considered as the origin of concentration polarization, especially above the water dissociation level or in the presence of electrochemically active species.[62] To prove this assumption for the present system, another experiment was carried out whereby the electrical potential drop over one electrode was kept below the water dissociation level of $\Delta\phi = 1.23$ V (Figure 4b, the potential difference over one electrode corresponds to 0.96 V). If Faradaic surface reactions are the reason for the concentration accumulation effect, no such effects should be observable below the threshold value since water dissociation was proven to be the only likely surface reaction. As evidenced by the quantitative fluorescent imaging data and the lateral concentration distribution of the electrolyte solution, also at an electrical field strength below the water dissociation threshold quite strong concentration effects become observable. Concentration effects not only are visible after single electrodes due to concentration polarization but also are substantially increased after the complete electrode array due to cooperative effects. Thus, the process of electrohydrodynamic demixing occurs despite the lack of surface reactions.

In conclusion, even if the existence of surface reactions at field strengths above the water dissociation level cannot be completely ruled out, the cyclic voltammetry data in combination with the imaging data at low electrical field strengths strongly support the assumption of capacitive charging as the physical origin of concentration polarization and the observed electrohydrodynamic demixing.

Design of the Microfluidic Demixers. These theoretical and practical considerations on nonlinear electrokinetics, surface electrochemistry, and the experimental realization of concentration polarization at a single electrode manifest that it is well possible to locally modify the bulk ionic concentration by nonlinear electrokinetics. To realize efficient demixing processes, the effects observed at the single-electrode level have to be combined via the devised architecture of an array of numerous electrodes. For this reason, different electrode array geometries were fabricated in otherwise straight and open microfluidic channels (Figure 5). As seen from the quantitative imaging data, symmetric arrays of electrodes seem to be rather unsuitable for the intended purpose of demixing. The zones of increased concentration polarization become deteriorated by the electrodes of the consecutive row. The upstreamly generated zone of increased concentration interacts at the frontal electrode surface with concentration polarization zones of negligible concentration effects. Therefore, the net effect on the bulk concentration distribution becomes deteriorated, and behind the array, the demixing effect is smaller than after the first row of electrodes. Despite strong concentration effects at the single-electrode level, this experiment results in the finding that the arrangement of the different electrodes within the array is of crucial importance.

To improve the array geometry, electrode ensembles are used that offer the aspects of a direction-oriented structure. This geometry is given if the electrodes are alternatingly tilted from one row to the next one by ±30° against the direction of the externally applied electrical field and, additionally, if the consecutive row is laterally shifted by several micrometers (cf. Figure 1b for an enlarged view of the design of the electrode array). Indeed, the fluorescence imaging data prove an effect on the total ionic concentration distribution (Figure 5). Again each single electrode polarizes the surrounding electrolyte. But the individual zones of increased and decreased ionic concentration overlap from one row of electrodes to the next one as an effect of the structure oriented electrode arrangement and the convective flow through device.

(62) Barany, S.; Mishchuk, N. A.; Prieve, D. C. *J. Colloid Interface Sci.* **1998**, *207*, 240−250.

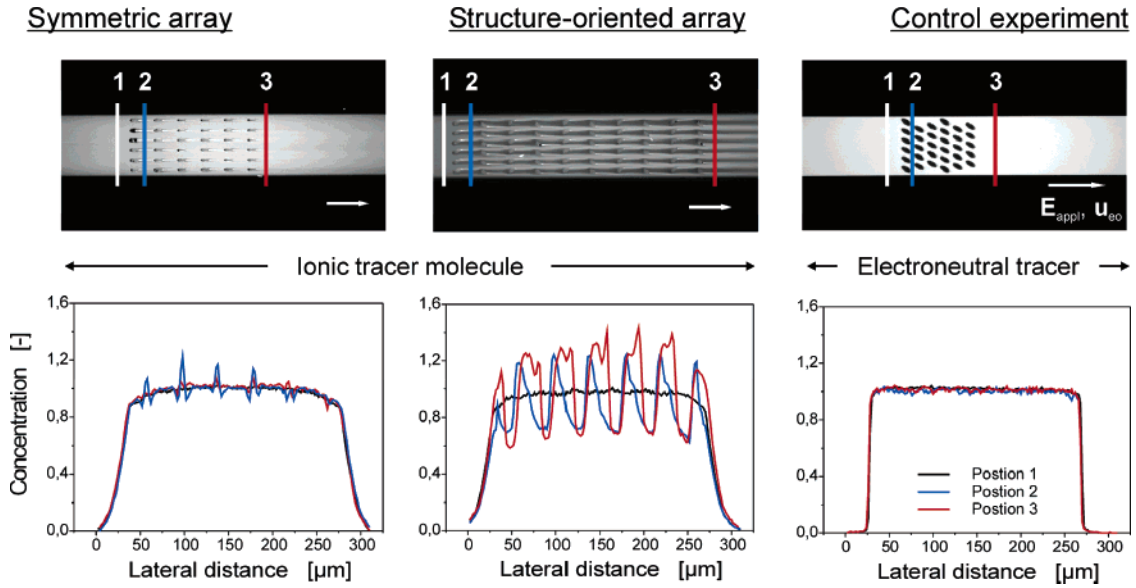

Figure 5. Fluorescent images and normalized lateral concentration profiles for different electrode array geometries but otherwise identical channel parameters and experimental conditions. The electrical field strength was 94 kV/m in all cases. The experimental conditions were similar to Figure 2. The concentration distribution was normalized to the mean electrolyte concentration in front of the array.

These electrohydrodynamic interactions between the concentration polarization at individual electrodes and the hydrodynamic flow finally lead to the desired demixing effect. An electrolyte solution of originally homogeneous ionic concentration can be separated into lateral laminae of increased and decreased ionic concentration whereby only axial electrical fields are applied.

Additional support for the above-described mechanism of electrohydrodynamic demixing comes from the control experiment with an electroneutral tracer molecule (also Figure 5). For this type of molecule, the applied external electrical fields and the field-induced space charges do not affect the local transport properties. Therefore, the concentration distribution remains homogeneous throughout the device. This experiment indicates that the demixing process is of electrohydrodynamic origin and affects only ionic molecules.

For a closer investigation of this process, the dependence of the demixing efficiency on the applied electrical field strength has to be quantified. As mentioned above, any process of demixing is characterized by a decrease of entropy due to the reduced number of possible microstates. Thus, the determination of the entropy change as a function of the applied electrical field strength not only explains the field dependency but additionally gives an estimate on the relative yield of the process. By referring the salt content within the laminae of the demixed solution to the reference states of pure substances, the entropy change during demixing calculates to[13]

$$\Delta_D S = -R(x_2 \ln x_2 - x_1 \ln x_1) \qquad (4)$$

with x_1 and x_2 denoting the average molar fraction of the electrolyte components in the streamlines of enriched and decreased ionic concentration as measured directly after the electrode array. By plotting the entropy change due to demixing against the applied electrical field strengths, a strong sigmoidal character becomes observable (Figure 6a). At low field strengths, hardly any effect is observed. However, if stronger electrical field strengths are superimposed, a sharp increase of the entropy change can be monitored above ~30 kV/m. It asymptotically approximates an entropy decrease of −1.1 mJ/(mol K). Compared to a complete demixing into streamlines of doubled and zero concentration with −3.3 mJ/(mol K) of entropy change, the observed demixing efficiency corresponds to 33% for the presented experimental conditions and microchip design.

At low electrical field strengths, the development of concentration polarization is rather small due to the reduced surface flux (cf. Figure 6b, where the fluorescence images and the corresponding lateral concentration profiles are given). Additionally, the electroosmotic flow velocity caused by the charged glass surface of the microfluidic device remains in the submillimeter per second range ($\mu_{eo,\,exp} = 4.5 \times 10^{-8}$ m^2/(V s)). This combination of reduced flow velocity and small ionic surface transport leads to concentration polarization of a rather small spatial extension with low intensity. Therefore, hardly any demixing effect can be detected downstream or even within the electrode array. At elevated field strengths above 30 kV/m, however, a sharp increase of the entropy change becomes visible until at relatively strong electrical fields the demixing process asymptotically approaches its maximum entropy reduction. The explanation of these experimental observations relies on the two different effects that promote the above-mentioned electrohydrodynamic interactions. First, the electrokinetic effect of concentration polarization becomes more pronounced at elevated field strengths. Second, the electroosmotic flow velocity increases to several millimeters per second, giving rise to a largely extended slipstream behind the electrodes until it reaches the next row of electrodes. Then, cooperative concentration effects between the different rows of electrodes become realized and continuously amplify the demixing process. The corresponding fluorescence images of the demixing process at low, moderate, and high electrical fields support these considerations. The convective flow transports the demixing further

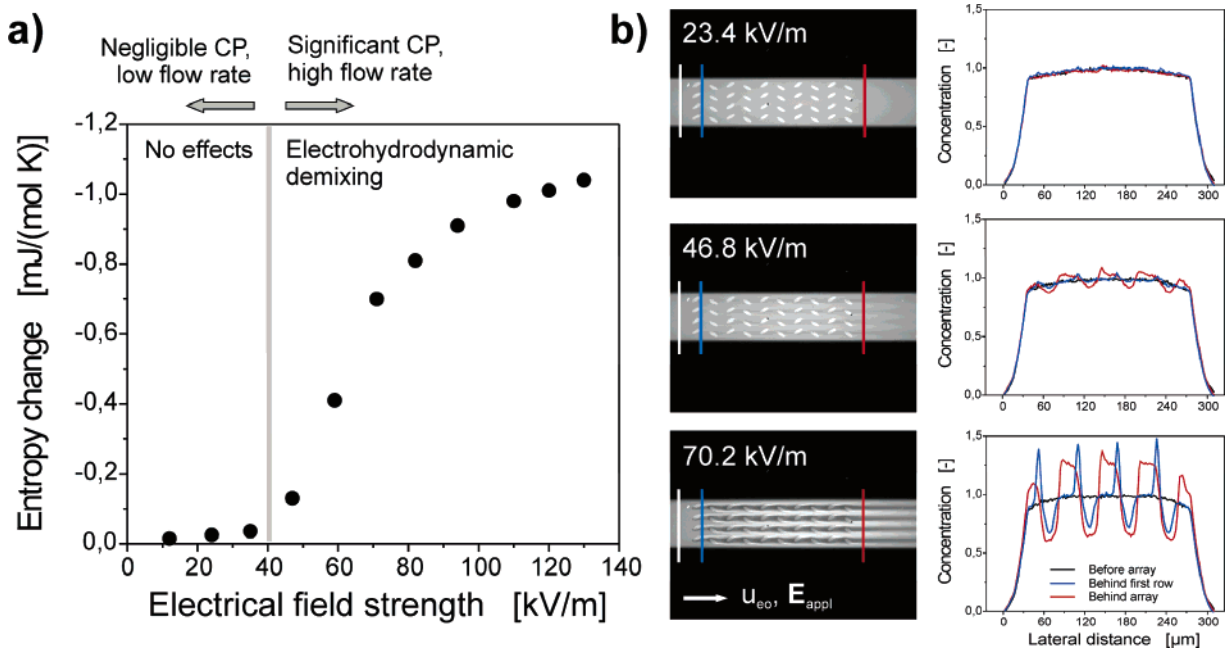

Figure 6. (a) Change of entropy of the demixing process vs electrical field strength. The difference in entropy of the homogeneous and demixed solution was calculated by referring the states before and after demixing against the reference state of pure compounds. The maximum entropy change for complete demixing yields -3.3×10^{-3} J/(mol K). (b) Fluorescence images of the ionic tracer distribution at steady state and the corresponding normalized lateral concentration profiles for different field strengths (experimental conditions as in Figure 2).

downstream, and if high Peclet numbers are realized, the electrolyte solution stays demixed far beyond the array.

The peculiarity of the above-presented demixing system is that the concentration accumulation and depletion of the incoming homogeneous solution is performed into laminae of increased and decreased ionic concentration. However, the different streamlines of identical concentration remain isolated from each other. To increase the net effect of concentration accumulation, the combination of different streamlines has to become possible. For this reason, a modification of the array structure was carried out. The electrode array was equipped with laterally extended electrodes whereby the axial dimension was kept constant to prevent Faradaic surface reactions and undesired air bubble formation. These electrodes then enable a direction-oriented displacement of individual concentrated laminae into combined streamlines of strongly increased ionic concentration in the middle of the channel as demonstrated by quantitative fluorescent imaging data (Figure 7). Obviously, the midstream concentration accumulation devices offer a substantially increased ionic concentration downstream the electrode array.

Interestingly, the net increase in the accumulated zones is more intensive than the decrease inside the depleted zones. A possible explanation of this observation is based on the physical properties of concentration polarization. This phenomenon characterizes a dynamic manipulation of the local ionic concentration distribution around regions with ion-selective transport properties. Inside concentration polarization zones, the mass flux by convection and electromigration can be considered to be strongly reduced.[57] In this context, the high concentration inside the polarization zones does not necessarily denote a large transport downstream the array (cf. the electrodes can be compared to concrete dams: the higher the dam, the higher the water level, but the amount of water that passes remains constant all along the river). The same takes place for the displayed data of midstream concentration. Depending on the ion permselectivity, the geometrical structure of the electrode, and the concentration of the surrounding electrolyte, the ionic concentration inside the polarization zone can be substantially altered. Consequently, the laterally extended electrodes show a polarization pattern different from that of their smaller counterparts. As indicated by the concentration profiles of Figure 7, there definitely exists a certain optimum lateral extension and tilting angle with respect to the applied field direction. Thus, these laterally extended electrodes show a much stronger lateral concentration manipulation. Additionally, due to their larger spatial extension, they are able to laterally shift the maximum of the ionic concentration to the midstream region. Thus, these electrodes are able to combine individual streamlines if the incoming electrolyte solution already exists as a demixed solution of laminae of increased concentration. After reaching the steady state, the whole electrolyte solution behind the electrode array finally shows a strongly increased electrolyte concentration. This experiment on laterally extended electrodes shows the possibility to arbitrarily pattern the concentration distribution and constitutes a major step toward an efficiently working (micro-) fluidic salt concentration device.

CONCLUSIONS

The presented electrohydrodynamic demixing process provides a conversion of fundamental aspects of nonlinear electrokinetics into applied microfluidics. The process takes advantage of the possibilities of freely structuring the microdevice geometry and combining different materials into the same microfluidic device. By equipping it with dedicated aspects of asymmetry, the structure-directed conversion of axial electrical energy input into lateral molecularly selective transport realizes the reversion of the diffusion-based process of mixing. Electrohydrodynamic demixing

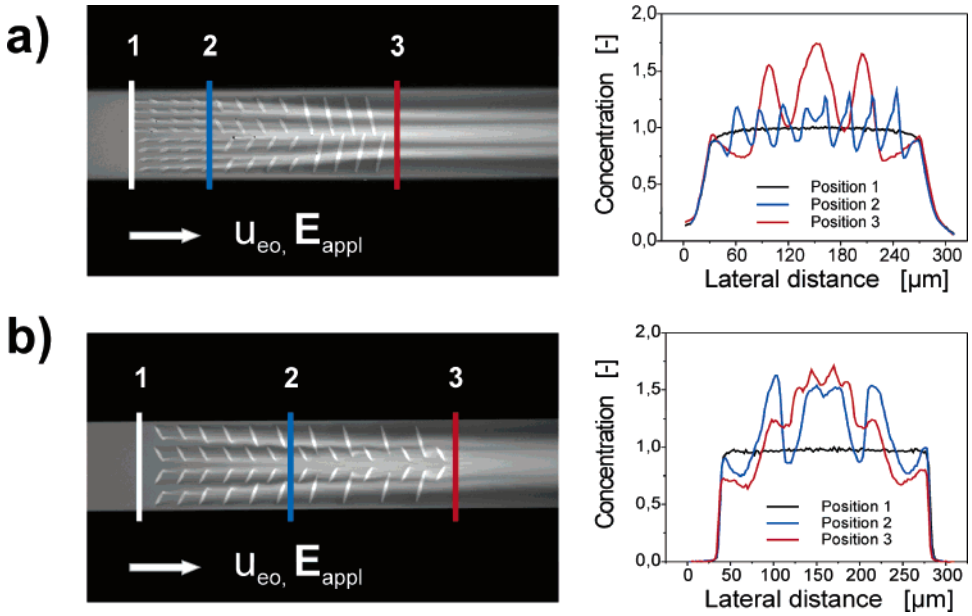

Figure 7. Fluorescence image and the corresponding lateral concentration profile for the midstream concentration accumulation of the electrolyte solution. Different laterally extended electrodes were used within the array to combine individual laminae of increased concentration (experimental conditions as in Figure 2).

and concentration accumulation of any type of electrolyte becomes possible. Applications of this complex process may be found in devices for enhanced detection sensitivity of microfluidics, in stand-alone concentration accumulation devices, or, if scaled-up successfully, in large-scale water purification or desalination systems. Additionally, the system could be turned into a continuous-flow separation system for ionic species of different electrophoretic mobility.

ACKNOWLEDGMENT

This work was supported by a NanoNed grant "Ion selection by electrical double layer effects" through the Dutch Ministry of Economic Affairs. The authors thank Sebastiaan Herber for his valuable contributions.

Received for review September 9, 2005. Accepted December 8, 2005.

AC051615N